Electronic Supplementary Material (ESI) for Nanoscale.
This journal is © The Royal Society of Chemistry 2021

Supporting Information

Correlating *in situ* RHEED and XRD to study Growth Dynamics of Polytypism in Nanowires

Julian Jakob,[*ab] Philipp Schroth,[abc] Ludwig Feigl,[b] Mahmoud Al Humaidi,[ac] Ali Al Hassan,[bc] Arman Davtyan,[c] Daniel Hauck,[b] Ullrich Pietsch,[c] and Tilo Baumbach[ab]

[*] *E-mail: julian.jakob@kit.edu*

[a] *Laboratory for Applications of Synchrotron Radiation, Karlsruhe Institute of Technology, Kaiserstrasse 12, D-76131 Karlsruhe, Germany.*

[b] *Institute for Photon Science and Synchrotron Radiation, Karlsruhe Institute of Technology, Hermann-von-Helmholtz-Platz 1, D-76344 Eggenstein-Leopoldshafen, Germany.*

[c] *Solid State Physics, Emmy-Noether Campus, Walter-Flex Strasse 3, D-57068 Siegen, Germany.*

1 Nanowire growth

The self-catalysed GaAs NWs were grown on n-type Si(111) substrates covered with native oxide in a custom designed MBE chamber dedicated for *in situ* XRD and RHEED experiments [2]. The substrates were first degassed for 30 min at T = 300°C before loading them into the growth chamber. To condition the substrate and control the number density of NWs, the SMP method presented elsewhere was used [4]. Before the actual NW growth at T_{sub} = 580°C (sample A), respectively T_{sub} = 590°C (samples B - F), we performed an additional step to the standard SMP method, where only Ga was deposited to form droplets on the substrate, with an equivalent thickness of 48 ML of planar GaAs at sample A and 40 ML of planar GaAs at samples B - F, respectively. After this predeposition step, self-catalysed GaAs NWs were grown by simultaneous supply of Ga and As_4 with an equivalent Ga-limited 2D layer growth rate of 0.1 ML/s and a V/III ratio of 3.5 (sample A) and a V/III ratio of 2.1 (samples B - F), respectively. For sample A, after t_A^{f1} = 30 min of NW growth, first the Ga supply was stopped while the As_4 flux was kept constant to consume the liquid Ga droplet at the tip of the NWs. For the other samples, both fluxes were stopped together after the respective growth time given in the article.
The fluxes were pre-calibrated by RHEED during the growth of GaAs layers on GaAs(001) substrates and the transitions of the (2x4) to the (4x2) surface reconstruction. The substrate temperature was calibrated by the GaO desorption temperature.

2 XRD experiments

The *in situ* XRD experiment of sample A was performed at the Resonant Scattering and Diffraction Beamline P09 [3] at the synchrotron facility PETRA III at DESY in Hamburg, Germany with a X-ray beam energy of 15 keV and a PILATUS 300K 2D detector. During the growth experiment we subsequently recorded small reciprocal space maps in the vicinity of the phase-selective zinc blende (311), the twinned zinc blende (220) and the wurtzite (10.3) Bragg reflections of the GaAs by scanning through each reflection with an overall temporal resolution of approximately 3.75 min and a slight time delay between the three subsequently recorded phase-sensitive reflections. This drawback is compensated by the advantage of a high Q-resolution giving access to the fine structure of the Bragg reflection patterns, allowing, *e.g.*, to distinguish radial from axial volume growth rates. Additionally, in each scanning cycle, the Si (311) Bragg reflection was measured as a reference. The beam size of 16(v) x 70(h) μm^2 allowed us to measure a large NW ensemble and to ensure gaining its mean properties. The experiment was completed by a post-growth RSM at room temperature with high-resolution. For samples B-F, we measured reciprocal space maps in the vicinity of the symmetric Si(111) and GaAs(111) reflections at the same beamline.

3 RHEED experiments

The RHEED setup of the MBE chamber consists of a SPECS RHD-30 gun which is run in our case at 20 keV. The 2D diffraction patterns on the fluorescence screen are captured with a low noise 14-bit PCO PixelFly camera with maximal time-resolution of 140 ms. During growth, every 7 second we recorded and integrated 5 frames of 140 ms exposure time resulting in a high temporal resolution. For the analysis of the phase-sensitive RHEED intensity spots, we integrate the intensities in the vicinity of each spot and correct for the background and structure factors of the reflections.

4 Correction of the XRD intensities for the CRY contribution

A remaining major problem in the growth of self-catalysed GaAs NWs on Si substrates, covered with a native oxide layer, is the simultaneous formation of GaAs in the non-catalytic growth mode (vapor-solid growth mode). These GaAs object are called parasitic crystallites and have typically aspect ratios close to one. They adopt only the zinc blende crystal structure (ZB and TZB) and form usually already at the onset of the growth run and thus can increase in volume over growth time.
Since both object types, NWs and CRY, consist of GaAs, their diffracted intensity overlap at the same position in reciprocal space. However, the CRY have a not so strict epitaxial connection to the substrate and show larger misorientation with respect to the substrate compared to the catalytic grown vertical NWs.
This feature allows the separation of both contributions in the XRD signals as shown in figure 1. The measured intensity distribution around the GaAs ZB(311) and GaAs TZB(220) reflections are a superposition of the NW and CRY contributions. In the left graph of figure 1, an exemplary RSM of the TZB(220) is depicted. For the correction of both ensemble contributions, we integrate the intensity perpendicular to the virtual Debye-Scherrer-ring, as indicated by the arrow. As a result, the profile in the right graph is obtained, with the experimental data shown in black. This signal can be fitted by two different contributions, a sharp one and a broader one with different center position. We identify the sharper one as the signal of the NWs because they are vertically well aligned and the broader one as the CRY contribution because of the worse epitaxial orientation on the substrate.
By repeating this procedure for all time-resolved RSMs, we obtain only the XRD intensity of the NW ensemble for our plots. In figure 2, we depict all measured data points of our *in situ* XRD experiment. After $t = 30$ min the intensity of all three crystal phases stays constant.

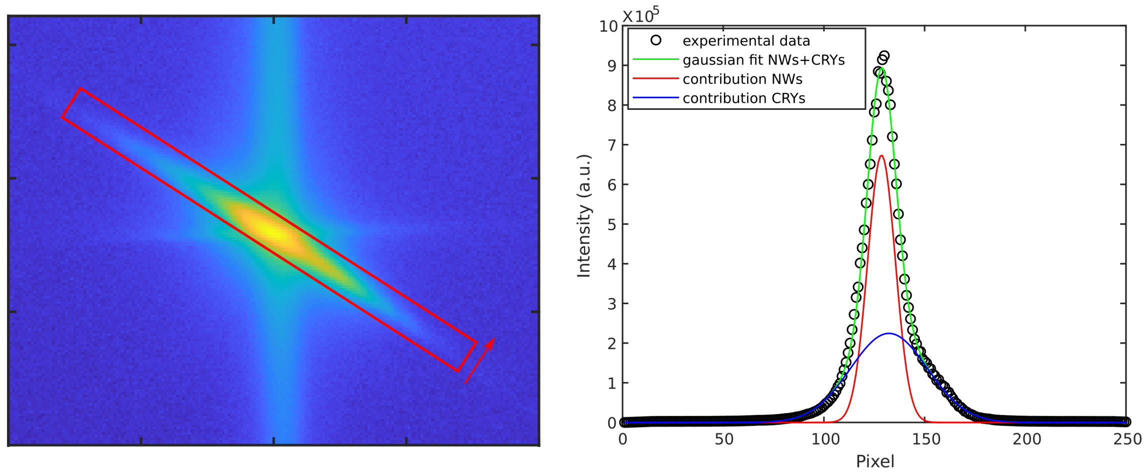

Figure 1: Reciprocal Space Map of the GaAs TZB(220) reflection (left). The intensity in the red box, summed up in the direction of the arrow, is plotted on the right. The experimental intensity (black) can be described by two Gaussian functions. The blue curve is interpreted as CRY contribution and the red one as NW contribution, both form the overall XRD signal (green).

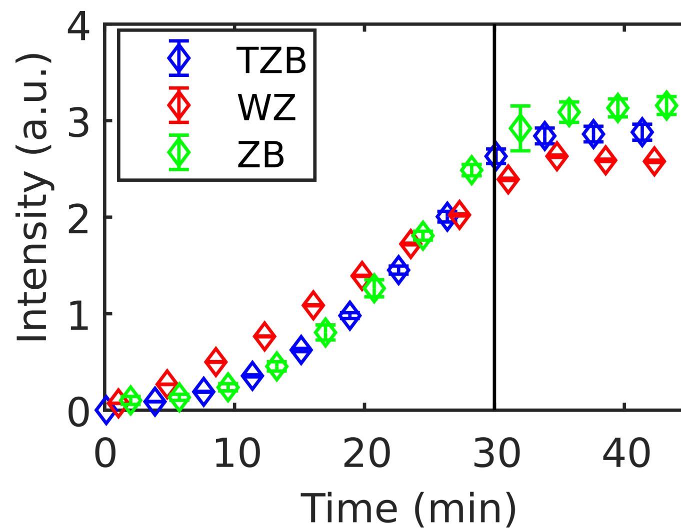

Figure 2: Temporal evolution of the phase-sensitive Bragg reflection intensities with additional captured data points (not shown in the manuscript), underlining the findings in the text.

5 Determination of the radial growth rate

We determined the radial growth rate at sample A by analysing the facet streaks perpendicular to Q_z in the XRD reciprocal space maps. In figure 3, an exemplary line profile along the facet streak of the WZ reflection at $t = 23.5$ min is depicted. For the analysis of the profile, we took into account that the NW ensemble of this sample shows a NW diameter distribution as we saw by post-growth SEM. Therefore, we convoluted the shape function of a NW with a certain radius with a Gaussian distribution. We use a standard deviation of 2 nm, which is motivated by the results of post-growth SEM. The resulting profiles are then compared with the experimental data.
In figure 3 the shape function of NWs with a mean NW radius of 19 nm convoluted with a standard deviation of 2 nm is depicted in red. The result is in good agreement with the experimental profile shown in black. For comparison, we additionally plotted the Q_y - profile of NWs with 19 nm radius and no diameter variation in blue. We directly see that neglecting the diameter distribution in the ensemble would lead to misinterpretation of the NW radii.

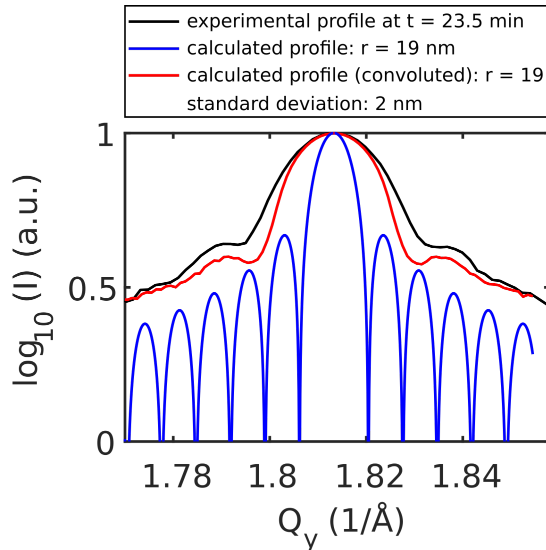

Figure 3: Q_y intensity profiles: the experimental Q_y - profile through the WZ reflection at $t = 23.5 min$ is shown in black, which fits well to the simulated Q_y - profile of a NW ensemble with mean NW radius of 19 nm and a Gaussian distribution of 2 nm, shown in red. For comparison a simulated Q_y - profile of a NW ensemble with mean NW radius of 19 nm and no diameter distribution is shown in blue.

6 RHEED and XRD simulations and post-growth SEM analysis

Details of the simulation and the related parameters can be found in Ref. [1]. The simulations were performed with a temporal resolution of t_i steps with the number i listed in table 1.
In a first simulation procedure, we simulated the intensity evolutions without polytypism and compared the resulting curves with the sum of the different polytypes of the experimental data: ZB+TZB+WZ. This allowed us to refine the structure parameters needed for the simulation model, like the NW number density ρ_{NW} and the initial NW radius r_0^{NW}. The final NW base radius $r_{f,b}^{NW}$, the final NW top radius $r_{f,t}^{NW}$, the final NW height h_f^{NW}, the crystallite number density ρ_{cry}, the final crystallite radius r_f^{cry}, and the final crystallite height h_f^{cry} were obtained by post-growth SEM. An exemplary SEM image of sample A is depicted in figure 4.
Each simulated intensity evolution for the different set of shape parameters were compared to the experimental intensity evolution of *in situ* RHEED and *in situ* XRD. The curves of the simulations as well as the obtained experimental data were normalized to equal areas, followed by the determination of the root-mean-square deviation (RMSD). The parameter set resulting in the curves with the lowest RMSD value describes the experiment the best.
In a second simulation, we now focussed on the polytype variation within the NW ensemble. Therefore, we used the phase-sensitive reflections and fixed the structure parameters to the parameters of the best result of the previous simulations. We now varied only the polytype distribution in the NW ensemble over a polytype fraction space. Again, we normalized the curves to equal areas, followed by the determination of the RMSD for WZ and ZB separately as well as for each diffraction method. The polytype distribution resulting in the intensity evolution with the lowest overall RMSD value, which means here the sum of the deviation of all curves (WZ and ZB of RHEED and WZ and ZB of XRD), is presented as the best description of the experimental data in figure 4 in the main article as black lines.
Table 1 summarizes the results of the SEM analysis of sample A, as well as the parameters used to run the simulations, resulting in the curves of figure 4 in the article. The table also summarizes the results of the SEM analysis of samples B - F, shown in figure 5 in the article, and the parameters used to run the simulations, obtaining the polytype fraction along the nanowire growth axis.

Table 1: Results of post-growth SEM analysis and parameters used for the simulations for samples A - F.

	sample A		sample B	
parameter	post-growth SEM	simulation	post-growth SEM	simulation
ρ_{NW} (μm^{-2})	8.4 ± 2.1	8.0	0.7 ± 0.2	0.7
r_0^{NW} (nm)	–	14	–	16
$r_{f,b}^{NW}$ (nm)	27 ± 2	27	16 ± 4	16
$r_{f,t}^{NW}$ (nm)	27 ± 2	27	19 ± 4	16
h_f^{NW} (nm)	800 ± 160	800	18 ± 4	20
ρ_{cry} (μm^{-2})	6.4 ± 2.0	6.0	–	0.9
r_0^{cry} (nm)	–	14	–	16
r_f^{cry} (nm)	80 ± 30	80	–	20
h_f^{cry} (nm)	100 ± 30	100	–	20
t_i	–	112	–	4
	sample C		sample D	
ρ_{NW} (μm^{-2})	1.0 ± 0.3	0.9	1.1 ± 0.3	0.9
r_0^{NW} (nm)	–	14	–	14
$r_{f,b}^{NW}$ (nm)	15 ± 2	16	16 ± 3	16
$r_{f,t}^{NW}$ (nm)	16 ± 2	16	16 ± 3	16
h_f^{NW} (nm)	66 ± 15	65	139 ± 44	120
ρ_{cry} (μm^{-2})	0.6 ± 0.2	0.8	0.9 ± 0.3	1.0
r_0^{cry} (nm)	–	14	–	14
r_f^{cry} (nm)	35 ± 14	35	53 ± 23	40
h_f^{cry} (nm)	32 ± 9	30	38 ± 10	55
t_i	–	25	–	40
	sample E		sample F	
ρ_{NW} (μm^{-2})	0.8 ± 0.3	0.6	0.8 ± 0.1	0.7
r_0^{NW} (nm)	–	14	–	14
$r_{f,b}^{NW}$ (nm)	21 ± 2	21	21 ± 3	20
$r_{f,t}^{NW}$ (nm)	22 ± 1	26	24 ± 2	23
h_f^{NW} (nm)	558 ± 123	550	829 ± 114	800
ρ_{cry} (μm^{-2})	0.3 ± 0.1	0.2	0.3 ± 0.1	0.2
r_0^{cry} (nm)	–	14	–	10
r_f^{cry} (nm)	82 ± 41	80	95 ± 66	85
h_f^{cry} (nm)	77 ± 30	90	95 ± 41	95
t_i	–	100	–	100

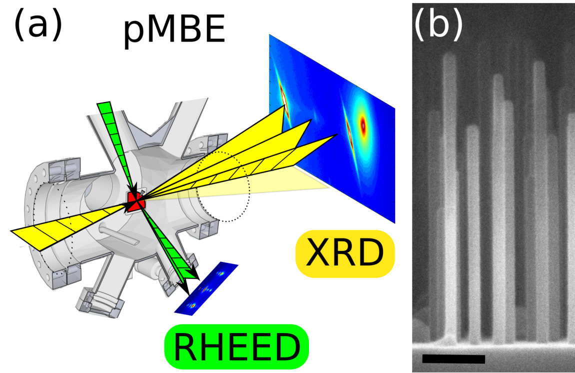

Figure 4: (a) Sketch of the experimental setup in the portable MBE chamber with the measurement geometries of RHEED and XRD. (b) Side view scanning electron micrograph of the GaAs NWs ensemble of sample A. The scale bar is 200 nm.

7 Effect of magnet field in synchrotron experimental hutch

In the experimental hutch of P09 at PETRA III, we observed instabilities of the RHEED experiment during the simultaneous *in situ* XRD and *in situ* RHEED experiment of sample A. We relate this issue to a magnetic field inside the experimental hutch. Since for the *in situ* XRD experiment, we moved the whole chamber on the diffractometer in order to excite different Bragg reflections, its relative position inside the hutch changed which might influence the electron beam. The instabilities of the RHEED signal coincide with these scans.
In absence of any magnetic field, which is the case in our home laboratory, the electron beam is stable and the intensity evolution doesn't show any instabilities, as depicted in figure 5.

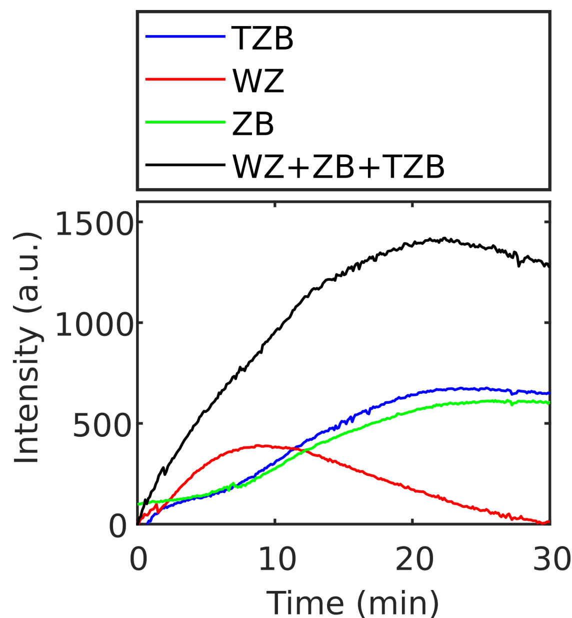

Figure 5: RHEED intensity evolution for a sample which was grown in our home laboratory. The intensity evolution doesn't show any instabilities underlining the effect of the magnetic field inside the experimental hutch during the experiment at the synchrotron.

References

[1] Jakob, J., Schroth, P., Feigl, L., Hauck, D., Pietsch, U., and Baumbach, T. Quantitative analysis of time-resolved rheed during growth of vertical nanowires. *Nanoscale 12* (2020), 5471–5482.

[2] Slobodskyy, T., Schroth, P., Grigoriev, D., Minkevich, A. A., Hu, D. Z., Schaadt, D. M., and Baumbach, T. A portable molecular beam epitaxy system for in situ x-ray investigations at synchrotron beamlines. *Review of Scientific Instruments 83*, 10 (2012), 105112.

[3] Strempfer, J., Francoual, S., Reuther, D., Shukla, D. K., Skaugen, A., Schulte-Schrepping, H., Kracht, T., and Franz, H. Resonant scattering and diffraction beamline P09 at PETRA III. *Journal of Synchrotron Radiation 20*, 4 (Jul 2013), 541–549.

[4] Tauchnitz, T., Nurmamytov, T., Hübner, R., Engler, M., Facsko, S., Schneider, H., Helm, M., and Dimakis, E. Decoupling the two roles of ga droplets in the self-catalyzed growth of gaas nanowires on siox/si(111) substrates. *Crystal Growth & Design 17*, 10 (Oct 2017), 5276–5282.